Reggeized model for η and η' photoproduction

Wen-Tai Chiang and Shin Nan Yang
Department of Physics, National Taiwan University, Taipei 10617, Taiwan

L. Tiator, M. Vanderhaeghen, and D. Drechsel
Institut für Kernphysik, Universität Mainz, 55099 Mainz, Germany
(Received 30 December 2002; published 8 October 2003)

A Reggeized model for η and η' photoproduction on the nucleon is presented. In this model, t-channel vector meson exchanges are described in terms of Regge trajectories to comply with the correct high energy behavior. We compare this Reggeized model with an isobar model (η-MAID), where the t-channel exchanges are described by ρ and ω poles. Both models contain the same resonance contributions, and describe current $\gamma p \to \eta p$ data up to $E_\gamma^{\rm lab}=2$ GeV quite well, but only the Reggeized model can be successfully extended to higher energies. For the $\gamma p \to \eta' p$ reaction, the Reggeized model is found to be able to give a satisfactory description. For the differential cross section data from SAPHIR, we find that the observed linear forward rise in cos θ near $E_\gamma^{\rm lab}=1.6$ GeV can be well described by the interference of an S_{11} resonance and the Regge trajectory exchanges without any need for an additional P-wave resonance.

DOI: 10.1103/PhysRevC.68.045202 PACS number(s): 13.60.Le, 14.20.Gk, 25.20.Lj, 25.30.Rw

I. INTRODUCTION

Photoproduction of η and η' on the nucleon, $\gamma N \to \eta N, \eta' N$, provides an alternative tool to study nucleon resonances (N^*) besides πN scattering and pion photoproduction. Both the ηN and $\eta' N$ states couple to nucleon resonances with isospin $I=1/2$ only. Therefore, these processes are cleaner and more selective to distinguish certain resonances than other processes, e.g., pion photoproduction. This provides the opportunity to access less explored nucleon resonances, especially some higher mass N^* about which only little information is as yet available.

During the last decade, the η photoproduction has been actively studied both theoretically and experimentally. The status was reviewed in our recent study [1]. On the other hand, the data on η' photoproduction are still very limited. In 1968, the ABBHHM Collaboration [2] observed 11 events in a bubble chamber using an untagged photon beam. With tagged photons an experiment at DESY in 1976 [3] found approximately seven η' candidates with a streamer chamber setup. In 1998 the SAPHIR Collaboration at Bonn [4] explored the energy region from 0.9 to 2.6 GeV with tagged photons and obtained angular distributions in seven energy bins. Unlike η photoproduction with an almost constant differential cross section in the threshold region, the η' photoproduction exhibits a sizable P-wave contribution from threshold to the maximum energy. In an isobar analysis the data could be well described by two resonances, S_{11} and P_{11}, at energies of $W=1897$ and 1986 MeV, respectively [4].

Among the theoretical studies on η' photoproduction, Zhang *et al.* [5] used a field theoretical Lagrangian model and explained the pre-1998 data of total cross sections well. Their calculations included Born terms, vector meson exchange, and resonance excitation, and strongly emphasized the $D_{13}(2080)$ excitation as the main production mechanism. Also Li [6] could give a good description of the total cross section data within a constituent quark model by generating nucleon resonances in the s channel. The dominant contribution was found from off-shell $S_{11}(1535)$ excitation. In a similar calculation in 2001, Zhao [7] could also well describe the SAPHIR data by introducing further P_{13} and F_{15} resonances. In both quark-model approaches, t-channel vector meson exchange was not included. In an equally good description of the data, Borasoy [8] applied U(3) baryon chiral perturbation theory with Born terms, vector mesons, and off-shell contributions from $P_{11}(1440)$ and $S_{11}(1535)$ resonances.

A very interesting subject in η and η' photoproduction is the meson coupling to the nucleon which determines the Born term contribution. Already in the SU(3) limit the coupling strength $g^2_{\eta NN}/4\pi=0.8-1.9$ is much smaller than for pions ($g^2_{\pi NN}/4\pi=14.3$), but in an analysis of the angular distributions of η photoproduction an even smaller value of $g^2_{\eta NN}/4\pi=0.4\pm0.2$ was determined [9]. Such a small value was later explained within a chiral Lagrangian approach [10,11], and in a very recent fit within a chiral constituent quark model a value of only 0.04 has been obtained [12]. For the η' coupling to the nucleon the situation is even less clear. Zhang *et al.* [5] applied a quark-model mixing relation with a singlet to octet mixing angle of $\theta=20°$ and obtained the relation $g_{\eta' NN} \simeq 0.7\, g_{\eta NN}$. From forward nucleon-nucleon scattering using dispersion relations, Grein and Kroll [13] estimated that both $g^2_{\eta NN}/4\pi$ and $g^2_{\eta' NN}/4\pi$ are smaller than 1, and in an analysis of the strangeness content of the proton Hatsuda [14] obtained values for the coupling constant in the range $-3 \leqslant g_{\eta' NN} \leqslant +2$ or $g^2_{\eta' NN}/4\pi \leqslant 0.7$.

Previously, we used an isobar model (η-MAID) [1] to study the η photoproduction and electroproduction on the nucleon, which described the experimental data quite well. Since both η and η' have the same quantum numbers, we expected that an extension of the η-MAID formalism to the η' photoproduction should be straightforward. However, this was not found to be the case. The reason for this problem turned out to be the much higher threshold for η' compared

to η production (W=1896 MeV vs W=1486 MeV). The approach used in the η-MAID model, which is intended for the resonance region at about $W \lesssim 2$ GeV, therefore has to be modified as the energy increases. The main modifications refer to the treatment of the t-channel contributions. The vector meson (e.g., ρ and ω) exchanges in the t channel are usually included in studies of meson photoproduction, and calculated by using Feynman (pole-like) propagators. As the energies increase, t-channel form factors are usually needed to regulate the t-channel contributions. However, at very high energies ($W \gg 2$ GeV) the use of meson poles in the t channel is found to fail.

On the other hand, it is well known that the Regge theory is successful in describing various reactions at high energy and low momentum transfer. In Ref. [15], the Regge trajectories in the t channel have been applied to pion and kaon photoproduction at high energies with success. Therefore, in this study we adapt a similar treatment for the t-channel vector meson exchanges and apply it to η and η' photoproduction.

In Sec. II, we describe the model ingredients, and focus on the Regge trajectory exchanges in the t channel. Our results and a comparison with both η and η' photoproduction data are given in Sec. III, followed by a summary and conclusions.

II. MODEL

Previously, we have used an isobar model (η-MAID) [1] to study the η photoproduction and electroproduction on the nucleon. This model contains Born terms, t-channel vector meson exchanges, and nucleon resonances. Although this model describes the current experimental data in the resonance region ($W \lesssim 2$ GeV) quite well, it cannot easily be extended to higher energies because of the vector meson poles used in the t-channel exchanges. To improve this situation, we adopt Regge trajectories to describe these t-channel exchanges. In the following sections, we first briefly introduce the resonance contributions and Born terms used in both models (details can be found in Ref. [1]); then we focus on the vector meson exchanges in the t channel.

A. Resonance contributions

For the resonance contributions of both the η-MAID and the Reggeized model, the relevant multipoles $\mathcal{M}_{\ell\pm}$ ($=E_{\ell\pm}, M_{\ell\pm}$) are assumed to have a Breit-Wigner energy dependence of the form

$$\mathcal{M}_{\ell\pm}(W) = \tilde{\mathcal{M}}_{\ell\pm}\, f_{\gamma N}(W)\, \frac{M_R \Gamma_{\rm tot}(W)}{M_R^2 - W^2 - i M_R \Gamma_{\rm tot}(W)}\, f_{\eta N}(W)\, C_{\eta N}, \tag{1}$$

where $f_{\eta N}(W)$ is the usual Breit-Wigner factor describing the ηN decay of the N^* resonance with total width $\Gamma_{\rm tot}$, partial width $\Gamma_{\eta N}$, and spin J,

$$f_{\eta N}(W) = \zeta_{\eta N} \left[\frac{1}{(2J+1)\pi} \frac{|\boldsymbol{k}|}{|\boldsymbol{q}|} \frac{M_N}{M_R} \frac{\Gamma_{\eta N}}{\Gamma_{\rm tot}^2} \right]^{1/2}, \tag{2}$$

with $|\boldsymbol{k}|$ and $|\boldsymbol{q}|$ the photon and η meson momenta in the c.m. system, and $\zeta_{\eta N} = \pm 1$ a relative sign between the $N^* \to \eta N$ and $N^* \to \pi N$ couplings.

The energy dependence of the partial width $\Gamma_{\eta N}$ is given by

$$\Gamma_{\eta N}(W) = \beta_{\eta N}\, \Gamma_R \left(\frac{|\boldsymbol{q}|}{|\boldsymbol{q}_R|} \right)^{2\ell+1} \left(\frac{X^2 + \boldsymbol{q}_R^2}{X^2 + \boldsymbol{q}^2} \right)^{\ell} \frac{M_R}{W}, \tag{3}$$

where X is a damping parameter for all resonances, assumed to be 500 MeV in the η-MAID and 450 MeV in the Reggeized model; Γ_R and q_R are the total width and the η c.m. momentum at the resonance peak ($W = W_R$), respectively, and $\beta_{\eta N}$ is the ηN decay branching ratio. The total width $\Gamma_{\rm tot}$ in Eqs. (1) and (2) is the sum of $\Gamma_{\eta N}$, the single-pion decay width $\Gamma_{\pi N}$, and the rest, for which we assume dominance of the two-pion decay channels,

$$\Gamma_{\rm tot}(W) = \Gamma_{\eta N}(W) + \Gamma_{\pi N}(W) + \Gamma_{\pi\pi N}(W). \tag{4}$$

The widths $\Gamma_{\pi N}$ and $\Gamma_{\pi\pi N}$ are parameterized similarly as for $\Gamma_{\eta N}$. More details about the parametrization of Eq. (1) can be found in Ref. [1].

In our previous study [1], we did not require the form factor $f_{\gamma N}(W)$ for the γNN vertex in the Breit-Wigner form, Eq. (1). However, we now found that it is necessary to include $f_{\gamma N}(W)$ to describe the data at $W > 2$ GeV. Therefore, we assume the form

$$f_{\gamma N}(W) = \left(\frac{|\,\boldsymbol{k}\,|}{|\,\boldsymbol{k}_R\,|} \right)^2 \left(\frac{X^2 + \boldsymbol{k}_R^2}{X^2 + \boldsymbol{k}^2} \right)^2 \tag{5}$$

in Eq. (1) for all N^*. For $S_{11}(1535)$ resonance, the factor $f_{\gamma N}(W)$ decreases its contribution at high energies, but affects very little near the $S_{11}(1535)$ resonance region. For other resonances, the differences caused by this factor are negligible.

B. Born terms

The nonresonant background contains the usual Born terms and vector meson exchange contributions. It is obtained by evaluating the Feynman diagrams derived from an effective Lagrangian. In the η-MAID model, the Born terms are constructed in the standard way, and the details can be found in Ref. [1]. In the Reggeized model, however, we do not include the Born terms. The reason is that the correct treatment for the u-channel nucleon exchange, together with the Reggeized t-channel vector meson exchanges, requires to also introduce the nucleon Regge trajectories. Because of the lack of high energy data at backward angles, it is currently difficult to determine this u-channel contribution. Since the coupling constants $g_{\eta NN}$ and $g_{\eta' NN}$ are small, the difference caused by the absence of the Born terms is negligible at low energies. Their effects become important only when the energies increase (see Fig. 5 and the discussion in Sec. III).

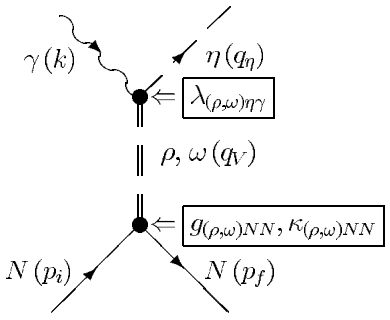

FIG. 1. The t-channel ρ and ω meson exchange diagram in η photoproduction.

C. Vector meson exchanges in the t channel

The Feynman diagram corresponding to t-channel vector meson ($V=\rho,\omega$) exchanges in η photoproduction is shown in Fig. 1. The electromagnetic coupling constants $\lambda_{V\eta\gamma}$ and $\lambda_{V\eta'\gamma}$ can be determined from the radiative decay widths,

$$\Gamma_{V\to\eta\gamma}=\frac{\alpha(m_V^2-m_\eta^2)^3}{24\,m_V^3\,m_\eta^2}\,\lambda_{V\eta\gamma}^2, \tag{6}$$

$$\Gamma_{\eta'\to V\gamma}=\frac{\alpha(m_{\eta'}^2-m_V^2)^3}{24\,m_V^2\,m_{\eta'}^3}\,\lambda_{V\eta'\gamma}^2, \tag{7}$$

where α is the fine-structure constant. In Table I, we list the values of $\lambda_{V\eta\gamma}$ and $\lambda_{V\eta'\gamma}$ as obtained from the widths of Ref. [16]: $\Gamma_{\rho\to\eta\gamma}$=36 keV, $\Gamma_{\omega\to\eta\gamma}$=5.5 keV, $\Gamma_{\eta'\to\rho\gamma}$=89 keV, and $\Gamma_{\eta'\to\omega\gamma}$=9.1 keV.

For the hadronic *VNN* vertex, a dipole form factor is included in the η-MAID. We choose the same form as in Ref. [1]: $(\Lambda_V^2-m_V^2)^2/(\Lambda_V^2+\boldsymbol{q}_V^2)^2$, with cutoffs Λ_ρ=1.0 GeV and Λ_ρ=1.3 GeV from our fit. However, this hadronic form factor is not required in the Reggeized model. Various values of the hadronic couplings g_{VNN} and κ_{VNN} can be found in the literature. Unlike the η-MAID where the values of the g_{VNN} and κ_{VNN} couplings are treated as fitting parameters, the Reggeized model contains these hadronic couplings as derived by a fit to high energy data, which will be discussed later in this section.

The adoption of Regge trajectories for vector meson (ρ and ω) exchanges allows us to describe the high energy behavior. More details about applying Regge trajectories for meson photoproduction can be found in Ref. [15], which deals with pion and kaon photoproduction at high energies.

The idea behind the replacement of the pole-like Feynman propagator by a Regge propagator, is to economically take into account the exchange of high-spin particles in the t (or u) channels which cannot be neglected any more as one moves to higher energies.

TABLE I. Parameters for the vector mesons in this study.

V	m_V (MeV)	g_{VNN}	κ_{VNN}	$\lambda_{V\eta\gamma}$	$\lambda_{V\eta'\gamma}$	$\alpha_V(t)$
ρ	768.5	2.4	3.7	0.81	1.24	0.55+0.8 t/GeV^2
ω	782.6	9	0	0.29	−0.43	0.44+0.9 t/GeV^2

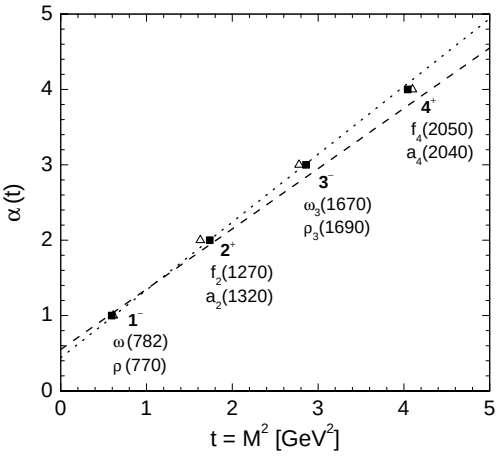

FIG. 2. Regge trajectories of the ρ and ω mesons shown by the dashed and dotted lines, respectively. Mesons belonging to the ρ (ω) trajectories are indicated by the symbols ■ (△).

The Regge trajectories are of the form $\alpha(t)=\alpha_0+\alpha' t$, where t is the Mandelstam variable, and shown in Fig. 2 for ρ and ω trajectories. The numerical values of α_0 and α' are taken from Ref. [15], and given in Table I.

$\rho(1^-)$ exchange:

$$\frac{1}{t-m_\rho^2}\Rightarrow\mathcal{P}^{\rho}_{\rm Regge} =\left(\frac{s}{s_0}\right)^{\alpha_\rho(t)-1}\frac{\pi\alpha'_\rho}{\sin[\pi\alpha_\rho(t)]}\frac{\mathcal{S}_\rho+e^{-i\pi\alpha_\rho(t)}}{2}\frac{1}{\Gamma(\alpha_\rho(t))}. \tag{8}$$

$\omega(1^-)$ exchange:

$$\frac{1}{t-m_\omega^2}\Rightarrow\mathcal{P}^{\omega}_{\rm Regge} =\left(\frac{s}{s_0}\right)^{\alpha_\omega(t)-1}\frac{\pi\alpha'_\omega}{\sin[\pi\alpha_\omega(t)]}\frac{\mathcal{S}_\omega+e^{-i\pi\alpha_\omega(t)}}{2}\frac{1}{\Gamma(\alpha_\omega(t))}. \tag{9}$$

The parameter s_0 is a mass scale taken as s_0=1 GeV^2, and $\mathcal{S}=\pm1$ is the signature of the trajectory. The Gamma function $\Gamma(\alpha(t))$ suppresses poles of the propagator in the unphysical region. As is well known from Regge theory [17], trajectories can be either non-degenerate or degenerate. A degenerate trajectory is obtained by adding or subtracting the two non-degenerate trajectories (corresponding in our case with 1^-, 3^-, 5^-, … and 2^+, 4^+, 6^+, … states, respectively, on the ρ or ω trajectories) with the two opposite signatures. This leads to trajectories with either a rotating ($e^{-i\pi\alpha(t)}$) or a constant (1) phase. In line with the finding of Ref. [15] for the ρ and ω trajectories, we use the rotating phase in the following. We further note that the Regge propagator reduces to the Feynman propagator $1/(t-m^2)$ if one approaches the first pole on a trajectory (i.e., $t\to m^2$).

Differential cross section data for $\gamma p\to\eta p$ at high s ($E_\gamma^{\rm lab}$=4 and 6 GeV) and low t (forward angles) were measured at DESY [18], as shown in Fig. 3. The data can be well described by the t-channel Regge trajectory exchanges. Fitting these data, we determine the values of the hadronic cou-

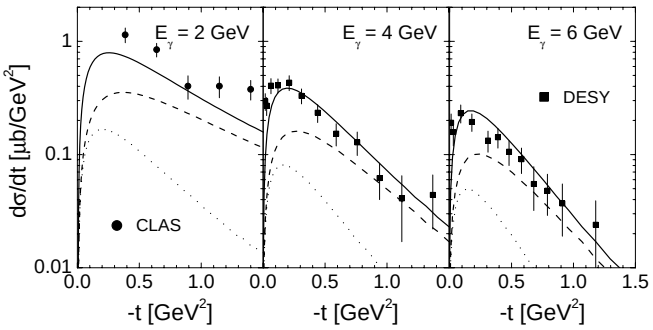

FIG. 3. Differential cross section $d\sigma/dt$ for $\gamma p \to \eta p$. The solid lines are the predictions from t-channel exchange using Regge trajectories, the dashed (dotted) lines indicate the $\rho(\omega)$ contributions only. The data at $E_\gamma^{\rm lab}$=4 GeV and 6 GeV are from DESY [18], at the lower energy we compare with the CLAS data [19] at $E_\gamma^{\rm lab}$ =1.925 GeV.

plings g_{VNN} and κ_{VNN}, as given in Table I. These values are then fixed and used for our calculation of both η and η' photoproduction.

III. RESULTS AND DISCUSSION

A. η photoproduction results

In this section, we present the η photoproduction results from the Reggeized model as well as the η-MAID model. The differences between the η-MAID results presented here and in Ref. [1] are that the former include the recent CLAS photoproduction data [19] in the fit. In the Reggeized model, we replace the t-channel ρ and ω exchanges used in η-MAID by the Regge trajectories while keeping the N^* contributions. Both models are fitted to current photoproduction data of cross sections from TAPS [20], GRAAL [21], and CLAS [19] as well as polarized beam asymmetry from GRAAL [22]. Note that we did not include the polarized target asymmetry measured at ELSA (Bonn) [23] in our fit for the reason discussed in Refs. [1,24].

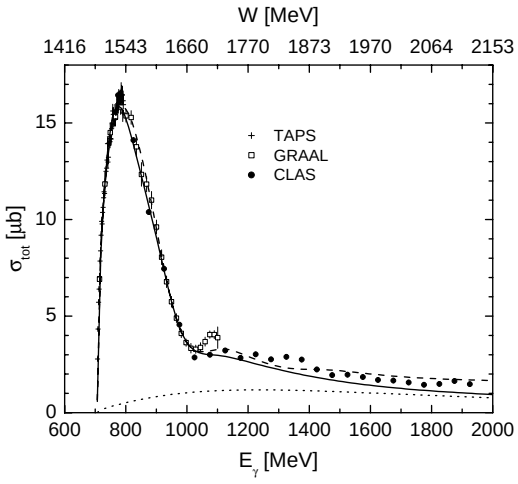

FIG. 4. Total cross section for $\gamma p \to \eta p$. The solid line is the full result from the Regge model, the dotted line indicates the contribution from t-channel Regge exchanges only. The η-MAID result is given by the dashed line. Data are from TAPS [20], GRAAL [21], and CLAS [19].

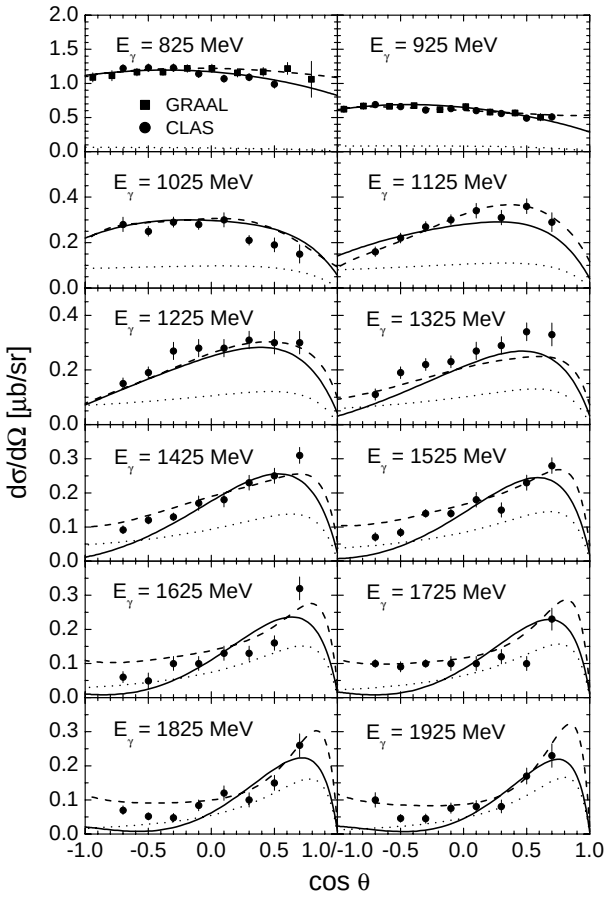

FIG. 5. Differential cross section for $\gamma p \to \eta p$. The data are from GRAAL [21] and CLAS [19]. Notation as in Fig. 4.

We show our result for the total cross sections in Fig. 4. Both models agree with the data quite well. Note that the GRAAL and CLAS total cross section data shown in Fig. 4 are given by integrating the respective differential cross sections. Since these measurements have certain limits on angular coverage, extrapolation to unmeasured regions is inevitable in order to estimate the total cross sections. Therefore, the obtained total cross sections depend on the extrapolation procedure. This explains that the bump seen in the GRAAL data near W=1.7 GeV ($E_\gamma^{\rm lab} \sim 1.1$ GeV) does not appear in the CLAS data. Both data sets agree on the differential cross sections, but because of the different extrapolations used, they deviate from each other for the total cross sections.

The results for the differential cross sections are given in Fig. 5. The overall agreement of the η-MAID results with the data is very good. The Reggeized model also agrees well with the data except for an underestimate at backward angles for $E_\gamma^{\rm lab} > 1.4$ GeV, which probably indicates the influence of the missing u channel. However, only the Reggeized model can be successfully extended to high energies, as is shown in Fig. 3 for $E_\gamma^{\rm lab}$=4 and 6 GeV. We note that the sharp decrease at forward angles for energies above 1 GeV is mainly due to the t-channel ρ and ω exchanges.

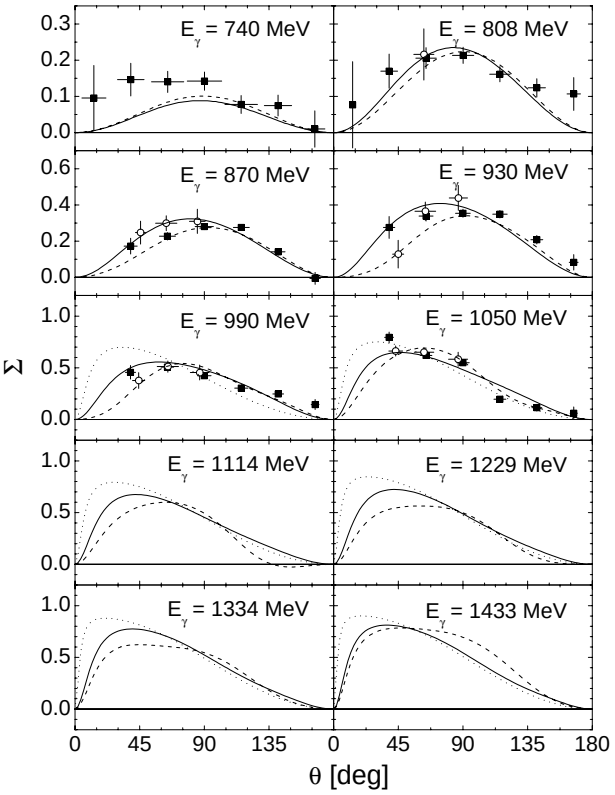

FIG. 6. Photon beam asymmetry Σ for $\gamma p \to \eta p$. Notation of the curves as in Fig. 4. Data are from GRAAL [22].

The results for the photon beam asymmetry are shown and compared with the GRAAL data [22] in Fig. 6. We also include the preliminary data from GRAAL [25] for $E_\gamma^{\rm lab}$ between 1.1 GeV and 1.5 GeV in our analysis, but those data are not shown here. Both models agree with the data reasonably well. Particularly in the Reggeized model, the forward-backward asymmetry at higher energies is naturally produced by the t-channel Regge trajectory exchanges. The large positive value of the photon asymmetry at high energies and forward angles indicates the dominance of the Regge exchanges in this region. Indeed at high s and $-t \ll s$, natural parity exchange (as in the case of ρ and ω Regge exchanges) leads to a photon asymmetry which approaches $+1$.

In Table II we present the nucleon parameters extracted from our fit using the Reggeized model. Among the nucleon resonances included in this study, we found that only the contributions from the $S_{11}(1535)$, $S_{11}(1650)$, and $D_{13}(1520)$ can be identified unambiguously by this reaction. The contributions from the other resonances are entangled near $W=1700$ MeV, and we find it difficult if not impossible to distinguish their individual contributions from the current η photoproduction data. Comparing with our previous η-MAID results [1], we find several resonances [e.g., $D_{15}(1675)$ and $F_{15}(1680)$] with much smaller $\beta_{\eta N}$ in the Reggeized model, implying that these resonance contributions become spurious and redundant once the t-channel exchanges have been Reggeized. Furthermore, the respective parameters should be cautiously interpreted, because several of them (e.g., Γ_R, $\beta_{\eta N}$, and $A_{1/2,3/2}$) are highly correlated.

TABLE II. Parameters of nucleon resonances studied in the Reggeized model. Masses and widths are given in MeV, $\zeta_{\eta N}$ give the relative sign between the $N^* \to \eta N$ and $N^* \to \pi N$ couplings, $\beta_{\eta N}$ are the partial decay branching ratios, and $A^p_{1/2,3/2}$ are the photoexcitation helicity amplitudes (in 10^{-3} GeV$^{-1/2}$). In the first row for each resonance, we list the average values or ranges given by the Particle Data Group (PDG) [26]. In the second rows the values are determined from our fitting; in case of no entry the PDG values are adopted.

N^*	Mass	Width	$\zeta_{\eta N}$	$\beta_{\eta N}$(%)	$A^p_{1/2}$	$A^p_{3/2}$
$D_{13}(1520)$	1520	120		0±1	−24±9	+166±5
			+1	0.04		
$S_{11}(1535)$	1520-1555	100-250		30−55	+90±30	
	1521	118	+1	50	+80	
$S_{11}(1650)$	1640-1680	145-190		6±1	+53±16	
	1635	120	−1	16	+46	
$D_{15}(1675)$	1670-1685	150		0±1	+19±8	+15±9
	1665		+1	0.7		
$F_{15}(1680)$	1675-1690	130		0±1	−15±6	+133±12
	1670		+1	0.003		
$D_{13}(1700)$	1700	100		0±1	−18±13	−2±24
			−1	0.03		
$P_{11}(1710)$	1680-1740	100		6±1	+9±22	
	1701		−1	26		
$P_{13}(1720)$	1720	150		4±1	+18±30	−19±20
			−1	4		

Therefore, these studies of η physics have to be combined with investigations of other channels or multichannel analyses to give reliable and convincing information about these resonances.

In conclusion, we find that both the η-MAID and the Reggeized model give an overall good description of the current data up to $E_\gamma^{\rm lab}=2$ GeV. ($\chi^2/N_{\rm dof}=2.0$ for the η-MAID and 3.9 for the Reggeized fit.) The Reggeized model shows some discrepancies at backward angles because the u channel is not included, but it is able to describe data at energies as high as $E_\gamma^{\rm lab}=6$ GeV , which are beyond the validity of the η-MAID model. It is not completely clear at which energy the Regge trajectories are necessary to describe the t channel. In our present study of η photoproduction, we find that Reggeization is not required for energies up to $W\sim 2$ GeV. However, the situation is different for η' photoproduction. For this reaction, we now show that the Regge trajectories are required even at energies already near the η' production threshold.

B. η' photoproduction results

The experimental data basis for η' photoproduction is still rather limited. Besides the total cross section data from AHHBBM [2] and AHHM [3] measured decades ago, the only modern data were obtained at SAPHIR (Bonn) [4]. However, this status will be largely improved by new data from CLAS, GRAAL, and CB-ELSA expected to come soon.

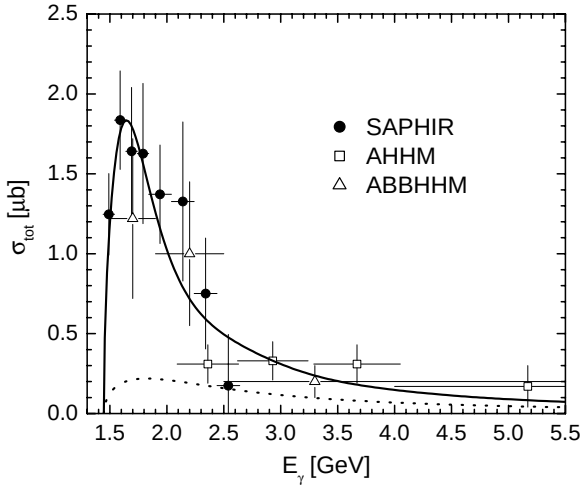

FIG. 7. Total cross sections for $\gamma p \to \eta' p$. The results are obtained by using Regge trajectories in the t-channel exchanges. The solid line shows the full results, and the dotted line indicates the t-channel contribution only. Data are from SAPHIR [4], AHHM [3], and ABBHHM [2].

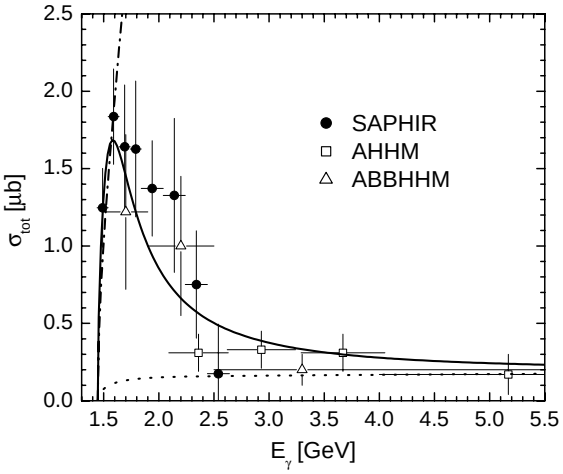

FIG. 8. Total cross sections for $\gamma p \to \eta' p$. These results are obtained by using ρ and ω poles in the t-channel exchanges, including hadronic form factors in the t channel. The solid line shows the full results, and the dotted line indicates the t-channel contribution only. The dash-dotted line indicates the full results without hadronic form factors in the t-channel. Data as in Fig. 7.

The vector meson couplings used in the t-channel exchanges are well determined: the photon couplings $\lambda_{(\rho,\omega)\eta'\gamma}$ can be obtained from the electromagnetic decay widths of $\eta' \to \rho\gamma$ and $\eta' \to \omega\gamma$ in Eq. (7), and for the strong couplings $g_{(\rho,\omega)NN}$ and $\kappa_{(\rho,\omega)NN}$ the same values as in η photoproduction are used. Furthermore, we find that the Born terms yield only small contributions because of the small $g_{\eta' NN}$ coupling suggested by various studies [5,13,14]. The current data are not able to determine such a small contribution, and thus we do not include the Born terms as in the case of η photoproduction. Therefore, the background contributions are completely fixed, and only resonance parameters are varied to fit the data.

In the total cross section of $\gamma p \to \eta' p$ (Fig. 7), we observe a sharp rise at threshold and a quick falloff with energy. This behavior, also seen in η photoproduction, should be due to a strong S-wave contribution, most likely a dominant S_{11} nucleon resonance. Therefore, we start with only one S_{11} nucleon resonance and t-channel Regge trajectory exchanges to describe the $\gamma p \to \eta' p$ reaction.

The SAPHIR [4] data contain the total and differential cross sections from near the threshold ($E_\gamma^{\rm lab}$=1.45 GeV) up to $E_\gamma^{\rm lab}$=2.44 GeV. The results of our Reggeized model for the total cross section are shown in Fig. 7, and found to agree well with the SAPHIR data, along with earlier data from AHHM [3] and ABBHHM [2].

We also attempt to describe the η' photoproduction by using the ρ and ω poles in the t-channel exchanges just as we did in the η-MAID model. It is shown in Fig. 8 that the contributions from ρ and ω pole exchanges without any hadronic form factors increase drastically above threshold. This can be partly improved by including hadronic form factors as shown in Fig. 8. The functional form of these hadronic form factors is taken the same as in the η-MAID, with cutoffs Λ_ρ=1.1 GeV and Λ_ρ=1.5 GeV from our fit. Although it is possible to obtain acceptable result for the total cross sections, this pole description fails to reproduce differential cross section data, which is discussed next.

In Fig. 9, we compare the results for the differential cross sections with the SAPHIR data [4] using Regge trajectories and ρ and ω poles in the t-channel exchanges. We also give a prediction at $E_\gamma^{\rm lab}$=4 GeV showing a pronounced forward peak, which is typical for ρ and ω Regge trajectories (and poles) at the higher energies. We observe that the SAPHIR data show a linear forward rise in cos θ at $E_\gamma^{\rm lab}$=1.59 and 1.69 GeV. Surprisingly, this P-wave behavior can be almost reproduced by our Reggeized model, which includes only one S_{11} resonance and t-channel exchanges, without introducing a P-wave resonance. The individual contributions from the S_{11} resonance and t-channel exchanges are also

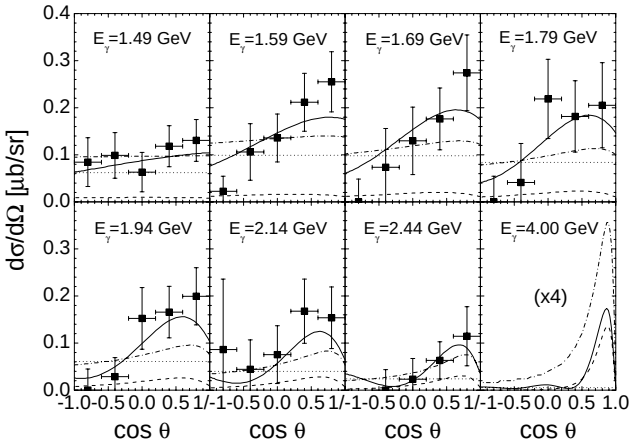

FIG. 9. Differential cross section for $\gamma p \to \eta' p$. The full results are given by the solid lines, and the dashed (dotted) lines indicate the contributions from the Reggeized t-channel exchanges (S_{11} resonance) only. The dash-dotted lines are the full results when using ρ and ω poles instead of Regge trajectories in the t-channel exchanges. Data are from SAPHIR [4].

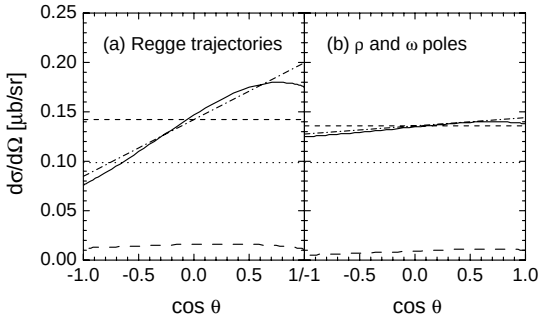

FIG. 10. The results for the differential cross section $\gamma p \to \eta' p$ at $E_\gamma^{\rm lab}=1.59$ GeV using (a) Regge trajectories and (b) ρ and ω poles in the t-channel exchanges. The full results are given by the solid lines, and the dotted (long dashed) lines indicate the contributions from the S_{11} resonance (t-channel exchanges) only. The dashed lines indicate the uniform angular contribution ($d\sigma_0$) only, while the dash-dotted lines also include the S-P wave interference term ($d\sigma_0+d\sigma_1$).

shown in Fig. 9, and both contributions have a nearly uniform angular distribution in the differential cross sections at these energies. Therefore, this linear behavior in cos θ is caused by a strong interference between the S_{11} resonance and t-channel Regge trajectory exchanges. This can be more easily understood if we expand the differential cross sections into a power series of cos θ,

$$\frac{d\sigma}{d\Omega}=\sum_{\ell=0}^{\infty} d\sigma_\ell=\frac{|\boldsymbol{q}|}{|\boldsymbol{k}|}\sum_{\ell=0}^{\infty} a_\ell \cos^\ell\theta, \tag{10}$$

where $d\sigma_\ell$ corresponds to the $\cos^\ell\theta$ term, and the angle-independent coefficients a_ℓ can be expressed in terms of multipoles. If we keep the S- and P-wave multipoles only and neglect higher partial waves, then a_1 is given as

$$a_1 = 2\ \mathrm{Re}[E_{0+}^*(3E_{1+}+M_{1+}-M_{1-})]. \tag{11}$$

Therefore, the linear behavior in cos θ for differential cross sections is basically the interference between the S- and P-wave multipoles.

However, this behavior is not reproduced by the model using the ρ and ω poles in the t channel, as this pole description gives almost flat differential cross section and fails to describe the data (see Fig. 9). The reason can be explained in Fig. 10, where we plot the $d\sigma_0$ and $d\sigma_1$ terms [defined in Eq. (10)] at $E_\gamma^{\rm lab}=1.59$ GeV using (a) Regge trajectories and (b) ρ and ω poles in the t-channel exchanges for comparison. It is clearly shown that these two models generate very different $d\sigma_1$ terms, resulting in very distinct differential cross sections. The pole description generates much smaller S- and P-wave interference because the amplitudes from the ρ and ω poles are real, and contain fewer higher partial waves. On the contrary, Regge trajectories generate complex amplitudes with more important contributions from higher partial waves. As the S_{11} resonance yields dominantly an imaginary contribution to the E_{0+} multipole around threshold, as can be seen from Fig. 14, the S-P wave interference of Eq. (11) is enhanced due to the imaginary part of the P-wave Regge multipoles.

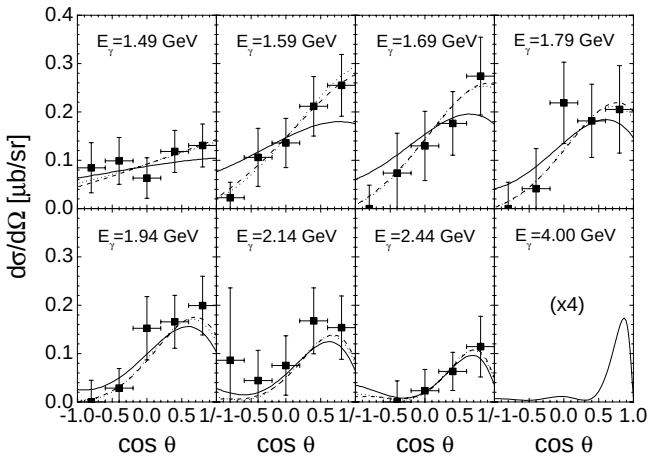

FIG. 11. Differential cross section of $\gamma p \to \eta' p$ for various N^* fits. The S_{11} plus Reggeized t-channel result is given by the solid line, and the result with an additional P_{11} (P_{13}) is indicated by the dashed (dotted) line. Data are from SAPHIR [4].

Therefore, our study shows that using Regge trajectories provides much better description for the η' photoproduction than using the ρ and ω poles. On the other hand, for the η photoproduction in the resonance region a pole description as used in the η-MAID model gives a satisfactory description. The pole description may be improved by introducing additional form factors depending on s. However, the inclusion of an s-dependent form factor in a t-channel exchange term would violate gauge invariance, and even so it would still eventually fail at the higher energies.

Although our model including only the S_{11} resonance and t-channel exchanges fits the data in terms of the overall χ^2 ($\chi^2/N_{\rm dof}=0.64$), the fit to the SAPHIR differential cross section data at $E_\gamma^{\rm lab}=1.59$ and 1.69 GeV can be improved by including an additional P-wave nucleon resonance. We find that both a P_{11} and a P_{13} resonance equally well improve the fit, as shown in Fig. 11. However, even a very precise cross section measurement cannot distinguish between a P_{11} or P_{13} resonance contribution without polarization measurements. In Fig. 12, we therefore give the predictions for the single-spin observables (T, P, Σ) and the beam-target double-spin observables (E, F, G, H). We find that the recoil polarization P is the most sensitive single-spin observable to P_{11} or P_{13} admixtures, and that the double-spin observables H shows equal sensitivity.

In Table III, we list the N^* masses extracted from the single S_{11} fit, and the fits with an additional P_{11} or P_{13} resonance. Although none of these resonances is well established, they are predicted by the constituent quark model and have been found in various analyses at $W=1.9-2.1$ GeV. In fact the Particle Data Group (PDG) lists $S_{11}(2090)$, $P_{11}(2100)$, and $P_{13}(1900)$ as one- or two-star resonances [26].

In our model discussed so far, we include the Reggeized t-channel exchanges as well as s-channel resonances. Phenomenologically, hadronic scattering amplitudes were found [27] to exhibit the property of duality, meaning that the amplitude can be obtained as a sum over s-channel resonances

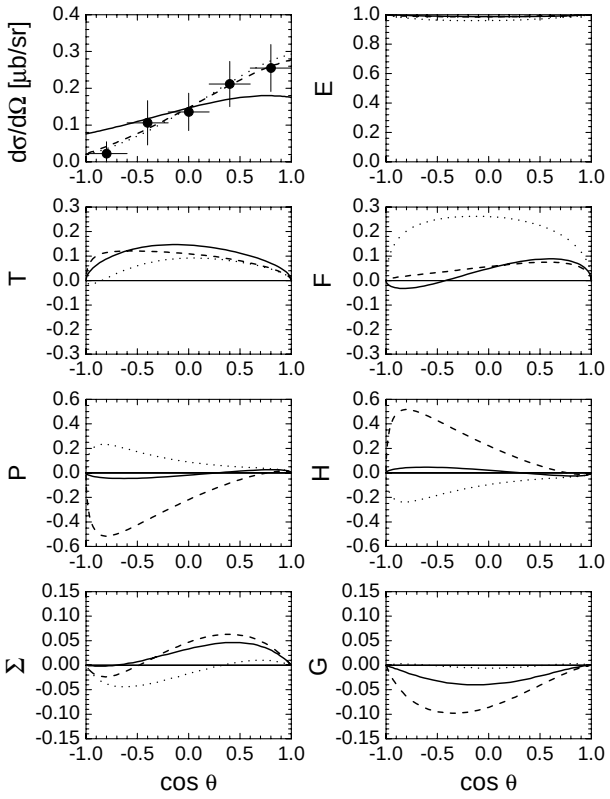

FIG. 12. Spin observables for $\gamma p \to \eta' p$ at $E_\gamma^{\rm lab}=1.59$ GeV for various N^* fits. The data are from SAPHIR [4]. Notation as in Fig. 11.

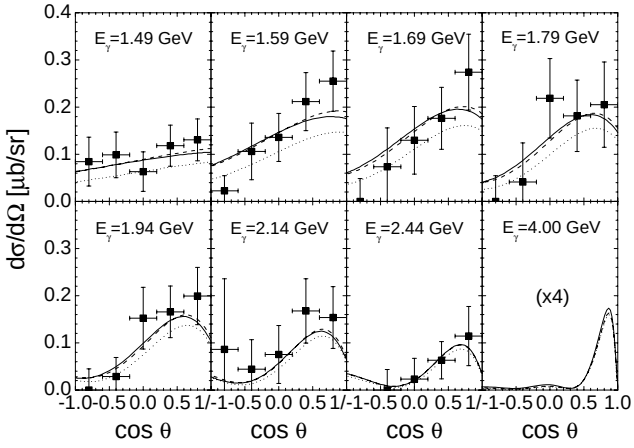

FIG. 13. Differential cross sections for $\gamma p \to \eta' p$. The solid line is the same as in Fig. 9. The dotted (dashed) line indicates the results obtained by removing the *S* wave from the *t*-channel Regge exchanges before (after) refitting the data. Data as in Fig. 9.

or as a sum over (*t*-channel) Regge pole exchanges. In particular, it has been shown quantitatively (e.g., for forward $\pi^- p \to \pi^0 n$ scattering) that these amplitudes satisfy finite energy sum rules, so that in the integral sense the sum over all *s*-channel resonances yields the same result as the sum over *t*-channel Regge poles, which is known as global duality. An addition of *s*-channel resonances and *t*-channel (Regge) exchanges therefore leads to some double counting. A pioneering model to implement this property of resonance-Reggeon duality for hadronic scattering amplitudes was proposed by Veneziano [28] and lead to many subsequent works. Such dual resonance models [29] were studied in quite some details and applied in a variety of processes, in particular, to meson-meson scattering amplitudes. For meson-baryon scattering or meson photoproduction, models based on the Veneziano model are usually too restrictive to give a realistic description of the scattering in the resonance region (as they imply strict relations between the coupling constants appearing in *s*-channel and *t*-channel processes). For an interesting dual amplitude model applied to πN scattering, which contains Regge asymptotic behavior for forward and backward angles and which shows resonance features at low energy, we refer to Ref. [30].

Without claiming that we solve the double counting problem and implement the property of duality, we study here as a first step a prescription to demonstrate the order of magnitude of double counting. In Fig. 13, we show the results when we completely remove the *S*-wave from the *t*-channel Regge trajectory exchanges at all energies. It appears that after refitting to the data, we essentially obtain the same results. Of course, the extracted resonance parameters are affected by this procedure.

Since several parameters (e.g., $A^p_{1/2}$, $\beta_{\eta N}$, and $\Gamma_{\rm tot}$) associated with these resonances are highly correlated among each other and cannot be well determined individually from current information, it is not appropriate to discuss the resonance parameters directly. Instead, we use the quantity

$$\xi = \sqrt{\frac{m_N k_R}{M_R q_R}\frac{\beta_{\eta' N}}{\Gamma_{\rm tot}}}\, A^p_{1/2}, \tag{12}$$

which is not sensitive to uncertainties for individual parameters and thus less model dependent. Using the parameter ξ, we find that its values before and after the refitting due to removing the *S* wave are 0.069 GeV^{-1} and 0.082 GeV^{-1}. Therefore, the increase of about 20% in ξ indicates the maximum degree of the double counting.

The E_{0+} multipoles predicted from our model are given in Fig. 14. We note that Regge exchanges yield a finite imagi-

TABLE III. Results of N^* masses extracted from various fits for $\gamma p \to \eta' p$.

Resonance fit	S_{11} mass (MeV)	P_{11} mass (MeV)	P_{13} mass (MeV)
S_{11}+*t*-channel	1959±35		
$S_{11}+P_{11}$+*t*-channel	1932±16	1951±32	
$S_{11}+P_{13}$+*t*-channel	1933±14		1954±37

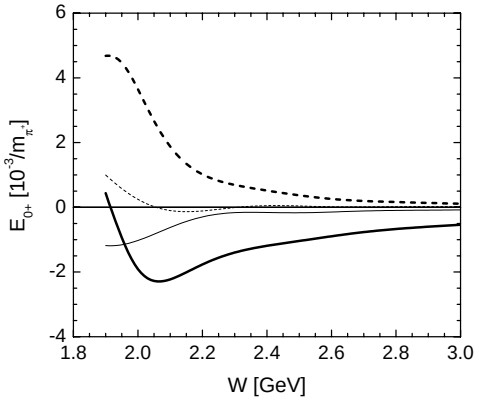

FIG. 14. E_{0+} multipoles (in $10^{-3}/m_{\pi^+}$) for $\gamma p \to \eta' p$. The thick lines are the full result, the thin lines correspond to Regge exchanges only. The real (imaginary) parts are indicated by solid (dashed) lines.

nary part of E_{0+}, while the pole exchanges in the t-channel always give real contributions. In Fig. 15 we also show the multipoles for the t channel Regge exchanges for $l \leqslant 5$.

IV. SUMMARY AND CONCLUSIONS

In this paper, we present a new study for η and η' photoproduction using a Reggeized model. This model contains resonance contributions along with Reggeized vector meson exchanges in the t channel, and yields a good description for these reactions in and beyond the resonance region.

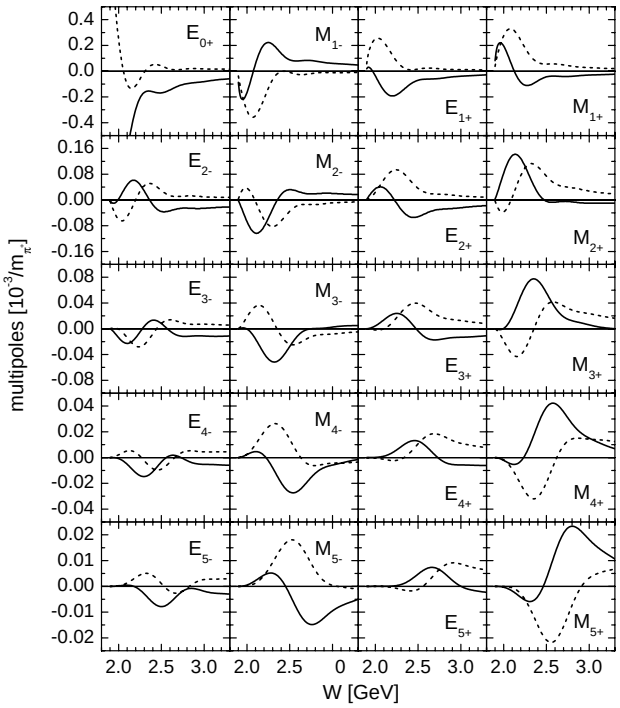

FIG. 15. Multipoles (in $10^{-3}/m_{\pi^+}$) for the t-channel Regge exchanges in the $\gamma p \to \eta' p$ process. Real (imaginary) parts are indicated by solid (dashed) lines.

We apply the Reggeized model to η photoproduction and compare our results with the η-MAID model, where ρ and ω poles are used instead. We find that both models allow us to achieve reasonably good fits of the current data from Mainz, GRAAL, and CLAS. Therefore, it is probably still appropriate to describe the t channel in terms of the ρ and ω poles in the resonance regions ($W \lesssim 2$ GeV). However, only the Reggeized model can be successfully applied to describe the high energy data of the DESY experiment at $E_\gamma^{\rm lab}=4$ and 6 GeV.

In the case of η' photoproduction, we find that its production threshold is too high to allow an acceptable description with vector meson poles in the t channel. Unlike the case of η photoproduction, the use of Regge trajectories is able to improve the description. Including only an S_{11} resonance and the Reggeized t channel, we are able to describe the current data. We find that most of the P-wave contributions are generated by the interference of a S_{11} resonance and ρ and ω Reggeized exchanges. In this study, we extract an S_{11} resonance with a mass in the range of 1932–1959 GeV, the exact value depending on whether or not an additional P-wave N^* is introduced. Though this procedure gives some evidence for such an S_{11} resonance, it does certainly not establish a resonance by itself. The PDG [26] lists the $S_{11}(2090)$ as a one-star resonance, and quotes previous results from Refs. [31–33], where the mass varies from 1880 to 2180 MeV. Recent analysis of pion-nucleon scattering and pion photoproduction [34] also indicates the existence of such a resonance. Furthermore, various quark models (e.g., Ref. [35]) have predicted an S_{11} resonance in this energy region. Therefore, the η' photoproduction provides a good channel to study this less explored resonance and possibly other higher-mass resonances as well.

Occasionally, a tendency of backward peaked η and η' differential cross sections was reported. Though this behavior has not been fully confirmed, it is likely due to the u-channel nucleon exchange and should be studied in future work by also introducing the nucleon Regge trajectories in the u channel.

The new forthcoming data for η and η' photoproduction and electroproduction will yield novel and interesting information on the nucleon resonance region. However, the analysis of these data in terms of nucleon resonances in the s-channel will require a consistent description of the observables over a large energy range and an improved treatment of the t- and u-channel backgrounds by means of Reggeized trajectories. The present work can serve as a first step in this direction.

ACKNOWLEDGMENTS

The authors would like to thank the members of the GRAAL and CLAS Collaborations for helpful discussions and for kindly sharing their data before publication. W.-T.C. is grateful to the Universität Mainz for the hospitality extended to him during his visits. This work was supported in parts by the National Science Council of ROC under Grant No. NSC91-2112-M002-023, the Deutsche Forschungsgemeinschaft (SFB 443), and a joint Project No. NSC/DFG TAI-113/10/0.

[1] W.-T. Chiang, S. N. Yang, L. Tiator, and D. Drechsel, Nucl. Phys. **A700**, 429 (2002).
[2] ABBHHM Collaboration, Phys. Rev. **175**, 1669 (1968).
[3] W. Struczinski *et al.*, Nucl. Phys. **B108**, 45 (1976).
[4] R. Plotzke *et al.*, Phys. Lett. B **444**, 555 (1998).
[5] J. F. Zhang, N. C. Mukhopadhyay, and M. Benmerrouche, Phys. Rev. C **52**, 1134 (1995).
[6] Z. Li, J. Phys. G **23**, 1127 (1997).
[7] Q. Zhao, Phys. Rev. C **63**, 035205 (2001).
[8] B. Borasoy, Eur. Phys. J. A **9**, 95 (2000).
[9] L. Tiator, C. Bennhold, and S. S. Kamalov, Nucl. Phys. **A580**, 455 (1994).
[10] M. Kirchbach and L. Tiator, Nucl. Phys. **A604**, 385 (1996).
[11] S. Neumeier and M. Kirchbach, Int. J. Mod. Phys. A **15**, 4325 (2000).
[12] B. Saghai and Z. Li, Eur. Phys. J. A **11**, 217 (2001).
[13] W. Grein and P. Kroll, Nucl. Phys. **A338**, 332 (1980).
[14] T. Hatsuda, Nucl. Phys. **B329**, 376 (1990).
[15] M. Guidal, J. M. Laget, and M. Vanderhaeghen, Nucl. Phys. **A627**, 645 (1997).
[16] D. E. Groom *et al.*, Eur. Phys. J. C **15**, 1 (2000).
[17] P. D. B. Collins, *An Introduction to Regge Theory and High-Energy Physics* (Cambridge University, New York, 1977).
[18] W. Braunschweig *et al.*, Phys. Lett. **33B**, 236 (1970).
[19] M. Dugger *et al.*, CLAS Collaboration, Phys. Rev. Lett. **89**, 222002 (2002).
[20] B. Krusche *et al.*, Phys. Rev. Lett. **74**, 3736 (1995).
[21] F. Renard *et al.*, Phys. Lett. B **528**, 215 (2002).
[22] J. Ajaka *et al.*, Phys. Rev. Lett. **81**, 1797 (1998).
[23] A. Bock *et al.*, Phys. Rev. Lett. **81**, 534 (1998).
[24] L. Tiator, D. Drechsel, G. Knöchlein, and C. Bennhold, Phys. Rev. C **60**, 035210 (1999).
[25] V. Kuznetsov *et al.*, GRAAL Collaboration, πN Newsletter **16**, 160 (2002).
[26] K. Hagiwara *et al.*, Phys. Rev. D **66**, 010001 (2002).
[27] R. Dolen, D. Horn, and C. Schmid, Phys. Rev. **166**, 1768 (1968).
[28] G. Veneziano, Nuovo Cimento A **57**, 190 (1968).
[29] P. H. Frampton, *Dual Resonance Models and Superstrings* (World Scientific, Singapore, 1986).
[30] J. W. Alcock, Y. A. Chao, and R. E. Cutkosky, Nucl. Phys. **84**, 503 (1975).
[31] D. M. Manley and E. M. Saleski, Phys. Rev. D **45**, 4002 (1992).
[32] R. E. Cutkosky *et al.*, Phys. Rev. D **20**, 2839 (1979).
[33] G. Höhler *et al.*. Handbook of Pion-Nucleon Scattering, Physics Data, Vol. 12-1, Karlsruhe, 1979.
[34] G.-Y. Chen *et al.*, Nucl. Phys. **A723**, 447 (2003).
[35] M. M . Giannini, E. Santopinto, and A. Vassallo, Nucl. Phys. **A699**, 308 (2002).